RESEARCH PAPER

Preparation and Characterization of NiO-WO_3 nanocomposite with Enhanced Photocatalytic Activity under Visible Light Irradiation

V. Ramasamy Raja [1], K. Muthupandi [1], A. Karthika [2], B. Aravindhan [3], L. Nithya [4]*

[1] *Department of Chemistry, Mannar Thirumalai Naicker College,Tamil Nadu, India*

[2] *Department of Chemistry, Latha Mathavan Arts and Science College, Tamil Nadu. India*

[3] *Department of Chemistry, The Madura College, Tamil Nadu, India*

[4] *Edustar Model School,Tamil Nadu, India*

ARTICLE INFO

Article History:
Received 10 December 2021
Accepted 27 February 2022
Published 01 April 2022

Keywords:
Crystal Violet
NiO/WO_3 nanocomposite
Photocatalytic activity
Visible Light

ABSTRACT

NiO/WO_3 nanocomposites has been successfully synthesized by a precipitation deposition method with different mole ratios were synthesized and characterized by Fourier transform infrared Spectra (FT-IR), X-ray diffraction (XRD), Energy dispersive X-ray spectroscopy (EDX), Scanning electron microscopy (SEM) and Transmission electron microscopy (TEM) techniques. Absorption range and band gap energy, which are responsible for the observed photocatalyst behavior, were investigated by UV-vis diffuse reflectance spectroscopy (UV-vis-DRS). The formation of cubic structured NiO and orthorhombic structured WO_3 was confirmed by powder X-ray diffraction analysis. The photocatalytic activity was tested for the degradation of Crystal Violet (CV) under visible-light irradiation. It was found that 0.5-0.5 mole NiO-WO_3 displayed excellent photocatalytic activity than that of 0.6-0.4 mole NiO-WO_3, 0.4-0.6 mole NiO-WO_3. The effect of operation parameters such as initial dye concentration, pH and catalyst concentration has been investigated in detail. The mechanisms of the enhancement of photocatalytic activity of the nanocomposite photocatalyst will be discussed by the p-n heterojunction principle and the valence band theory. The pure nanocomposite systems have been also reported for a comparative purpose.

How to cite this article
Rajaa V R., Muthupandi K., Karthika A, Aravindhan B., Nithya L. Preparation and Characterization of NiO-WO_3 nanocomposite with Enhanced Photocatalytic Activity under Visible Light Irradiation. J Nanostruct, 2022; 12(2):353-365.
DOI: 10.22052/JNS.2022.02.012

INTRODUCTION

In the recent years, environmental issues have become increasingly more important.Crystal violet (CV) dye is triphenylmethane cationic dye [1-2]. This is extensively used in industries such as textile/dyeing, ballpoint pen, paper, leather, additives, foodstuffs, cosmetics, fertilizers, antifreeze, detergents, leathers and analytical chemistry. On the other hand, advanced oxidation processes (AOPs) such as microwave catalysis, photocatalysis, membrane technique and advanced oxidants are promising in CV decolourization, it is important to efficiently remove such dyes for efficient environmental remediation. Photocatalysis for the purification of wastewater from industries and households has attracted much attention in recent

* *Corresponding Author Email: ramasamychem1989@gmail.com*

years [3-5].

NiO is wide band gap energy of (E_g = 3.5 eV, p-type semiconductor) frequently used as a cocatalyst loaded with different photocatalysts because the loading process is simple and inexpensive, and the photocatalysts loaded with NiO exhibited higher efficiencies for photocatalytic water splitting. Besides excellent electronic and optical properties, NiO also possess high chemical stability, super conductance characteristics, excellent electron transfer capability, and remarkable anti-inflammatory properties [6-8]. A large number metal oxides such as mixed nanometal oxide materials have been recognized in the past decade years, however among a wide range of metal oxides, Previous studies has been discussing the combination of NiO/Bi_2O_3 [9], NiO/$InVO_4$ [10], NiO/ZnO [11],NiO/TiO_2 [12].

WO_3, as an important n-type semiconductor with a band gap of 2.4 to 2.8eV, has been extensively used in many fields due to its unusual physical and chemical properties.Taking into account its strong adsorption within the solar spectrum, stable physicochemical properties as well as its resilience to photo corrosion, WO_3 is generally considered as a feasible candidate for construction of composite photocatalysts play an essential role in influencing light absorption and photocatalytic performances [13-15]. Among these methodologies, the construction of composite system with two different semiconductor photocatalysts is likely to possess superior photocatalytic performances, credited to higher charge-separation efficiency and restricted recombination rate of the photogenerated charge carriers. In the past years, WO_3 based on coupled semiconductors WO_3/g-C_3N_4 [16], WO_3/Fe_2O_3 [17],WO_3/Bi_3O_4Cl [18] has been studied.

In thepresent study, to prepare the NiO-WO_3nanocomposites with different NiO:WO_3 mole ratios were synthesized by the precipitation deposition method.The mole ratio between WO_3 and NiO was varied in order to obtain the most suitable composite material used for further application as photocatalyst. The structural and morphology of the synthesized samples were characterized using UV-Vis-DRS, FTIR, XRD, SEM, TEM, while the activity was evaluated for their adsorption performance for CV dye in aqueous solution. The factors influencing the photocatalytic performance and possible mechanism were discussed in detail.

MATERIALS AND METHODS

Materials

All the chemicals employed were of analytical grade and applied without further purification. Deionized water was employed in all experiments

Synthesis of NiO nanoparticle

$Ni(NO_3)_2.6H_2O$ is dissolved in concentrated HNO_3 (10 ml) and diluted to 100 ml with deionized water. The metal solution was hydrolyzed with stoichiometric amount of KOH by drop wise addition of a 1M solution under continuous stirring. The synthesis was carried out in polypropylene (PP) apparatus to avoid the possible contamination by silica from glass apparatus. The co-gel of $Ni(OH)_2$ was filtered, dried in hot air oven at 120ºC for 6h.

Synthesis of WO_3 nanoparticle

The WO_3 nanoparticles were synthesized under hydrothermal condensations. Experimental details were as follows: 10 g Na_2WO_4-$H_2O$was dissolved in 250 mL of distilled water. Then, the solution of 3 M HNO_3 was added drop wise into the above solution under continuous stirring until tungstenic acid was precipitated thoroughly. After that, tungstenic acid precipitate was collected, washed with deionized water and ethanol several times and dried in air at 100°C. 1 g tungstenicacid was dissolved in 45 mL deionized water and then transferred into Teflon–lined autoclave with a capacity of 100 mL. The autoclave weresealed and maintained at 110°–170 °C for 12 h. The solid precipitate was filtered and then dried at 100 °C for 2 h followed by calcination at 400 °C for 4 h.

Synthesis of NiO/WO_3 nanocomposites

The synthesized NiO powder was subsequently added to the WO_3precipitate (1:1.5). The pH of the prepared suspension was adjusted to 7by slowly adding 0.1 M of NaOH solution. The solution was transferredinto Teflon-lined stainless steel autoclave and hydrothermal reactionwas carried out at 120 °C for 6 h. Finally, NiO/WO_3 nanocompositeswere obtained from centrifugation and drying at 80 °C for 24 h.

Characterization

The UV-Vis-DRS was recorded on an UV-2450 spectrophotometer (Shimadzu Corporation, Japan) using $BaSO_4$ as the reference. Surface structure was characterized by XRD pattern obtained on X- ray diffractometer (XPERT PRO) with Cu Kα radiation at 25°C was used to determine

the crystallite size. Scanning electron microscopy (SEM) observations were performed by means of a JSM 6701F-6701 instrument in both secondary and backscattered electron modes. The elemental analysis was detected by an energy dispersive X-ray spectroscopy (EDX) attached to the SEM. Transmission electron microscopy (TEM) and selected area electrondiffraction (SAED) pattern were performed on a JEOL JEM-2100 electron microscope with anaccelerating voltage of 200 kV. Photodegradation experiments were performed in a HEBER immersion type photoreactor (HIPR-MP125).

Photodegradation Experiments

Photodegradation experiments were carried out in a cylindrical immersion type photoreactor. The photocatalytic activity was evaluated by monitoring the degradation of dyes under visible light irradiation.300ml aqueous solution of dye was taken in a cylindrical glass vessel equipped with a circulating water jacket to cool the lamp and to maintain constant temperature, in which air was bubbling continuously from the bottom of the reactor. Then, pH of the solution was adjusted using 0.1M H_2SO_4 (or) 0.1M NaOH and required amount of photocatalyst was added into the vessel. Before irradiation, the aqueous suspension containing EY and photocatalyst was continuously stirred for 30 min in dark to reach an adsorption-desorption equilibrium. After that, the mixture was subjected to visible light irradiation using 150W tungsten lamp. At regular time intervals, 5 ml aliquot of the reaction mixture was collected, centrifuged and filtered through a 0.2 µm to millipore filter to remove the photocatalyst powder. Then the filtrate was analyzed by UV-visible spectrometer to evaluate the residual EY concentration.

$$Percentage\ of\ photodegradation = \frac{(C_0 - C)}{C_0} X\ 100$$

Here C is the absorption of CV solution at irradiation time of 't' min. and C_0 is the initial absorption at t = 0 min.

RESULTS AND DISCUSSION

Optical absorbance analysis

The DRS of the as-prepared samples is shown in Fig. 1a. NiO nanoparticles have strong absorption peaks at 700nm and WO_3 nanoparticles with an absorption edge around 470nm in the visible light region.The observed redshift in 0.6-0.4 mole NiO-WO_3, 0.4-0.6 mole NiO-WO_3,0.5-0.5 mole NiO-WO_3nanocompositescan be attributed to the electron–hole transition between NiO and WO_3. The above result indicates that dispersing NiO on the WO_3 surface leads to the enhanced absorption in the visible light range,therefore, these NiO-WO_3 nanocompositeswould be promising for photocatalysis application [19-20].The enhanced light absorption may lead to formingmore electron–hole pairs. The optical energy band gap of the nanocomposites was measured using the Tauc relation. Abruptly, similar UV-vis absorption curves wereobserved and the absorption edges were calculated using the formula.

$$\alpha hv = A(hv - E_g)^{n/2} \quad (2)$$

Where, α, h, ν, A, E_g are the absorption coefficient, Planck'sconstant, incident light frequency, proportionality constant, and band gap energy respectively.The obtained bandgap energy values of NiO, WO_3,0.6-0.4 mole NiO-WO_3, 0.4-0.6 mole NiO-WO_3 and 0.5-0.5 mole NiO-$WO_3$are found to be 3.6eV, 2.59eV, 3.22eV, 2.98 and 2.72eV respectively and it is displayed in Fig. 1b. Hence 0.5-0.5 mole NiO-WO_3absorbs more visible light than that of NiO, WO_3.

Using the DRS results, the band edge positions of the nanocomposites were calculated theoretically using Mulliken electronegativity theory following the empirical equations 3 and 4.

$$E_{VB} = X - E_e + 0.5\ E_g \quad (3)$$

$$E_{CB} = E_{VB} - E_g \quad (4)$$

Where E_{VB} is the valence band edge potential, E_{CB} is the conduction band edge potential, E_g isthe band gap energy of the semiconductor, E_e is the scale factor of the hydrogen reference electrode (-4.5 eV), and χ is the absolute electronegativity of the semiconductor, which isdefined as the geometric mean of the absolute electronegativities of the constituent atoms. The calculated band edge potentials of the CB and VB of NiO and WO_3 are given in Table 1.

FT-IR Spectrum

The components of as-prepared composite catalysts were further confirmed by FT-IR. Fig. 2 showed the FT-IR spectra for NiO/WO_3 composites. The peaks at 3641 cm^{-1}, 3609 cm^{-1} and 3137 cm^{-1} are assigned to the stretching vibrations of OH

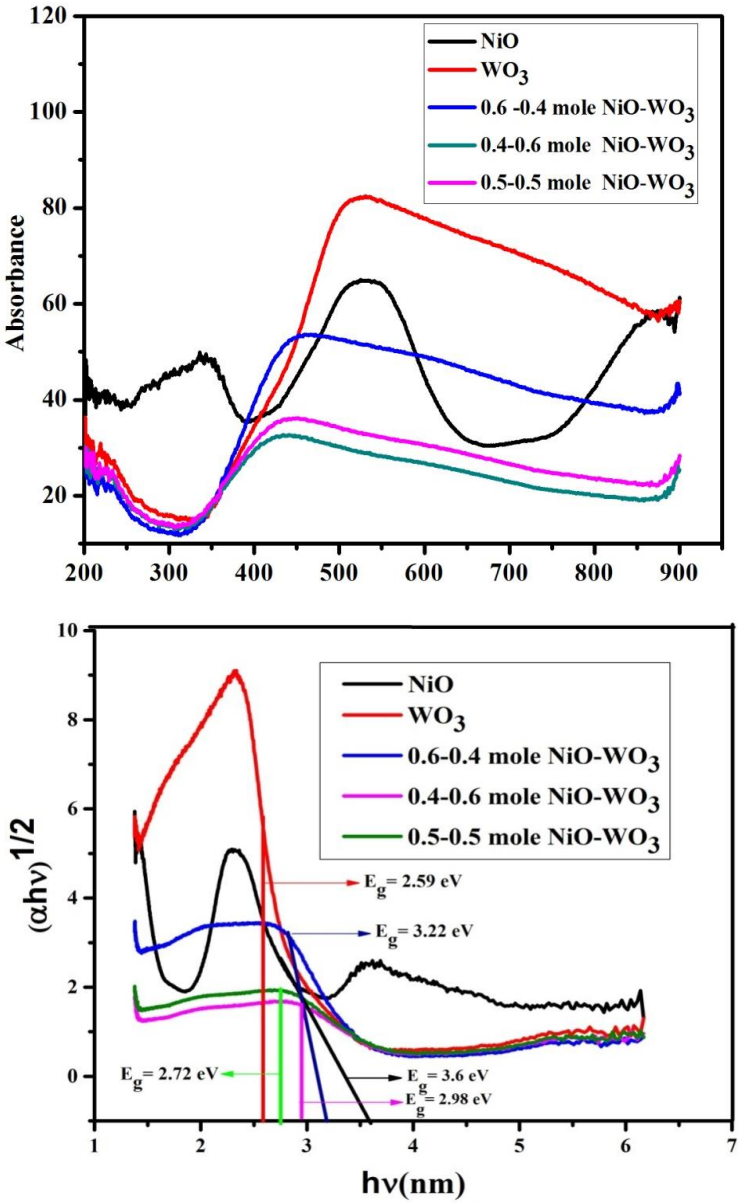

Fig. 1. (a) UV-Vis-DRS of NiO,WO_3, 0.6-0.4 mole NiO-WO_3, 0.4-0.6 mole NiO-WO_3, and 0.5-0.5 mole NiO-WO_3 (b) $(\alpha E_{photon})^{1/2}$ Vs E_{photon} curve of NiO ,WO_3 , 0.6-0.4 mole NiO-WO_3 , 0.4-0.6 mole NiO-WO_3, and 0.5-0.5 mole NiO-WO_3

Table.1.Estimated band-gap energies (Eg) and calculated EVB and ECB of NiO, WO_3

Catalyst	Absolute electronegativity X(eV)	Calculated conduction band position E_{VB} (eV)	Calculated valence band position E_{CB}(eV)	Energy band gap Eg (eV)
NiO	5.78	0.55	3.05	3.6
WO_3	6.59	0.79	3.38	2.59

group which is contributed by water contents. The vibrational band around 1624 cm^{-1} is due to the deformation vibration of H_2O molecule. The band ascribed to asymmetric stretching of C=O

is observed at 1403 cm^{-1}. The band at 1246 cm^{-1} is due to CO-C stretching vibrations. It can be clearly seen that the main characteristic peaks of pure NiO sample [21-22]. An intense broad band observed at 3442 cm^{-1} is owing to W-OH stretching vibration and can be ascribed to intercalation of H_2O. A peak located at 1640 cm^{-1} is assigned to the W–OH bending vibration mode of the adsorbed molecules of water. The peak at 1402 $cm^{-1}$was observed in the spectra of the terminal of vibrations W=O groups that were changed from the W-O bond on the surface of WO_3 or in the grain boundaries.The characteristic absorption bands of NiO and WO_3 were shifted to lower frequency in curve confirmed the association betweenthem. The above IR characteristic results have revealed the format ion and present of the NiO-WO_3 nanocomposite that is also confirmed by the XRD results as discussed below [23-24].

X-ray diffraction

The crystalline phases of composite sample were detected by XRD analysis. Fig. 3 exhibits the XRD patterns of NiO, WO_3 and NiO-WO_3 nanocomposite proportions. For NiO peaks observed at 2θ values 25.1º, 27.5º, 33.5º and 45.7º were respectively indexed as (0 1 2),(1 0 4), (1 1 0) and (2 0 0).It could be found that the NiO sample was well consistent with the structure of cubic phase (JCPDS No: #14-0688), and the WO_3 diffraction peaks matched with its orthorhombic phase at 30.1º,32.6º, 35.3º,45.4º,53.9º,60.5º and 65.9º were respectively indexed as indexed as (1 0 0),(0 2 0),(1 0 1),(1 0 2),(1 1 0), (1 0 3) and (2 0 1) (JCPDS No: # 46-1096). This suggests that WO_3 dispersed wellon theNiO surface. The crystallite sizes are calculated by the Debye-Scherrer equation. Theaverage crystallite sizes of NiO, WO_3, 0.6-0.4 mole NiO-WO_3, 0.4-0.6 mole NiO-WO_3,0.5-0.5 mole NiO-WO_3nanocompositesare 25.15 nm, 28.45nm, 33.09nm, 35.56 and 39.54nm respectively [25-26].

Morphological Investigations

The detailed morphology and microstructure of the pure NiO, WO_3, 0.5-0.5 mole NiO-WO_3 were investigated by SEM and EDAX. Fig. 4 (a), (b) and (c) the morphology of the pure NiO shows sand like structure, WO_3 shows candy with smooth surface structures, 0.5-0.5 mole NiO-WO_3 appears

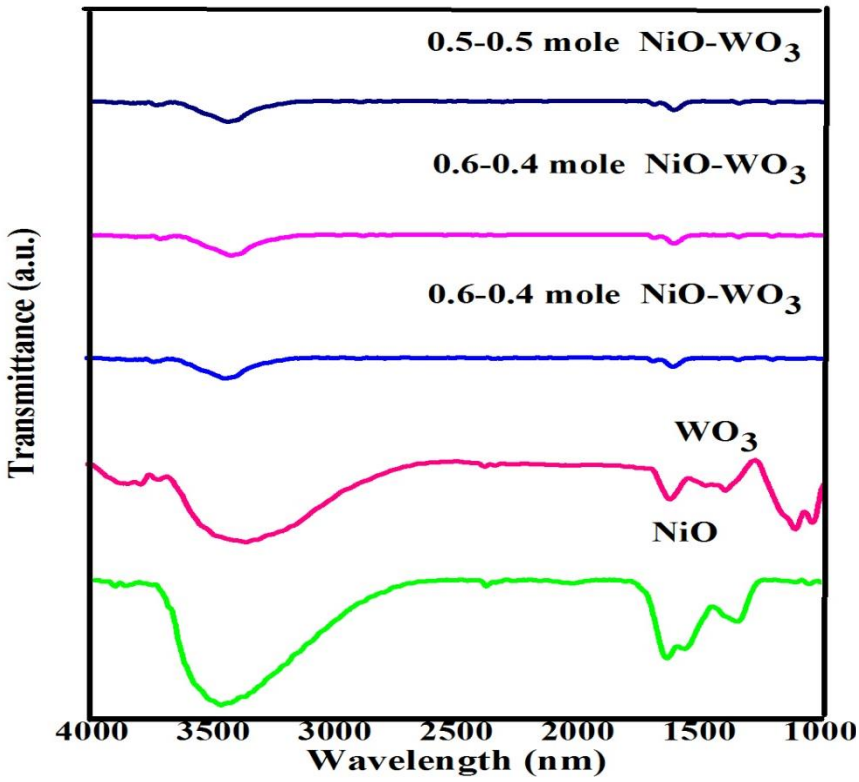

Fig. 2. FT-IR spectrum of NiO, WO_3, 0.6-0.4 mole NiO-WO_3, 0.4-0.6 mole NiO-WO_3, and 0.5-0.5 mole NiO-WO_3

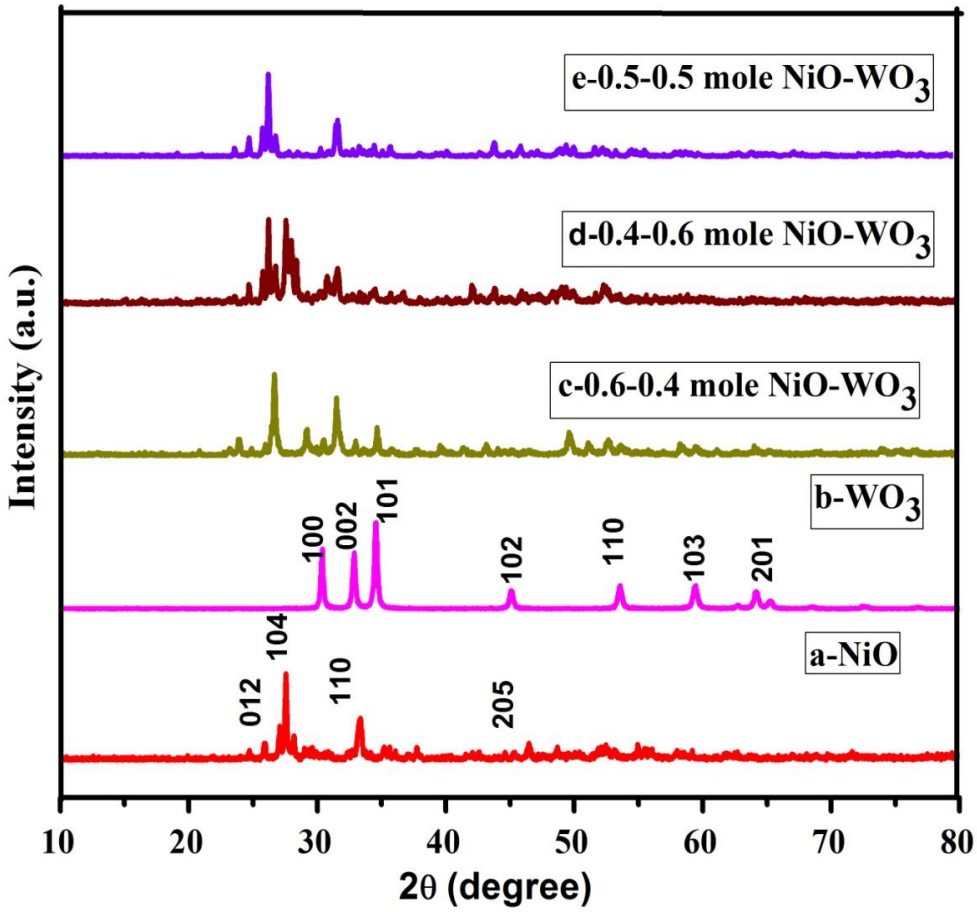

Fig. 3. XRD Pattern of (a) NiO (b) WO_3 (c) 0.6-0.4 mole NiO-WO_3 (d) 0.4-0.6 mole NiO-WO_3 (e) 0.5-0.5 mole NiO-WO_3

to be small spherical structure and the average particle size is below 25 nm. The EDAX shows the presence of elements such as Ni, W, and O in 0.5-0.5 mole NiO-WO_3composites as show in Fig. 4 (d).

The TEM measurement was performed in order to get detailed information about the crystalline structure of the photocatalyst. TEM image of 0.5-0.5 mole NiO-WO_3 nanocomposite is shown in Fig. 5(a). It can be seen from the figure that the average grain diameter of 0.5-0.5 mole NiO-WO_3 is around 21 to 47 nm. When the calcination was carried out at 80°C, as-prepared composite underwent a number of physical and chemical processes. The removal of water in the structure, including the adsorbed, intercalated and hydroxyl water, open up pore space and results in the formation of mesoporous structures. The corresponding diffraction rings and bright spot on the selected area electron diffraction (SAED) pattern Fig. 5 (b)suggest that the 0.5-0.5 mole NiO-WO_3 nanocomposite obtained are highly crystalline in nature, which is also consistent with XRD results [27]. The Fig. 5 (c) presents the HRTEM image of the 0.5-0.5 mole NiO-WO_3 composite, the clear lattice fringes reveal that the materials are highly crystallized. Different lattice images are observed with d spaces of 0.21nm corresponding to the (2 0 0) plane of cubic NiO, and with d spaces of 0.30nm belongs to the (0 2 0) plane of orthorhombic WO_3, respectively. The HRTEM analysis demonstrated that the existence of 0.5-0.5 mole NiO-WO_3 nanocomposite. These results are in good accordance with the XRD results [28].

Photocatalytic activity

Photodegradation of CV

The photocatalytic activity of NiO-WO_3 samples was tested by the degradation of CV under visible-light irradiation at room temperature. CV is very difficult to be decomposed for its chemically stability and it shows a maximum adsorption peak at 565nm. Fig. 6 shows the

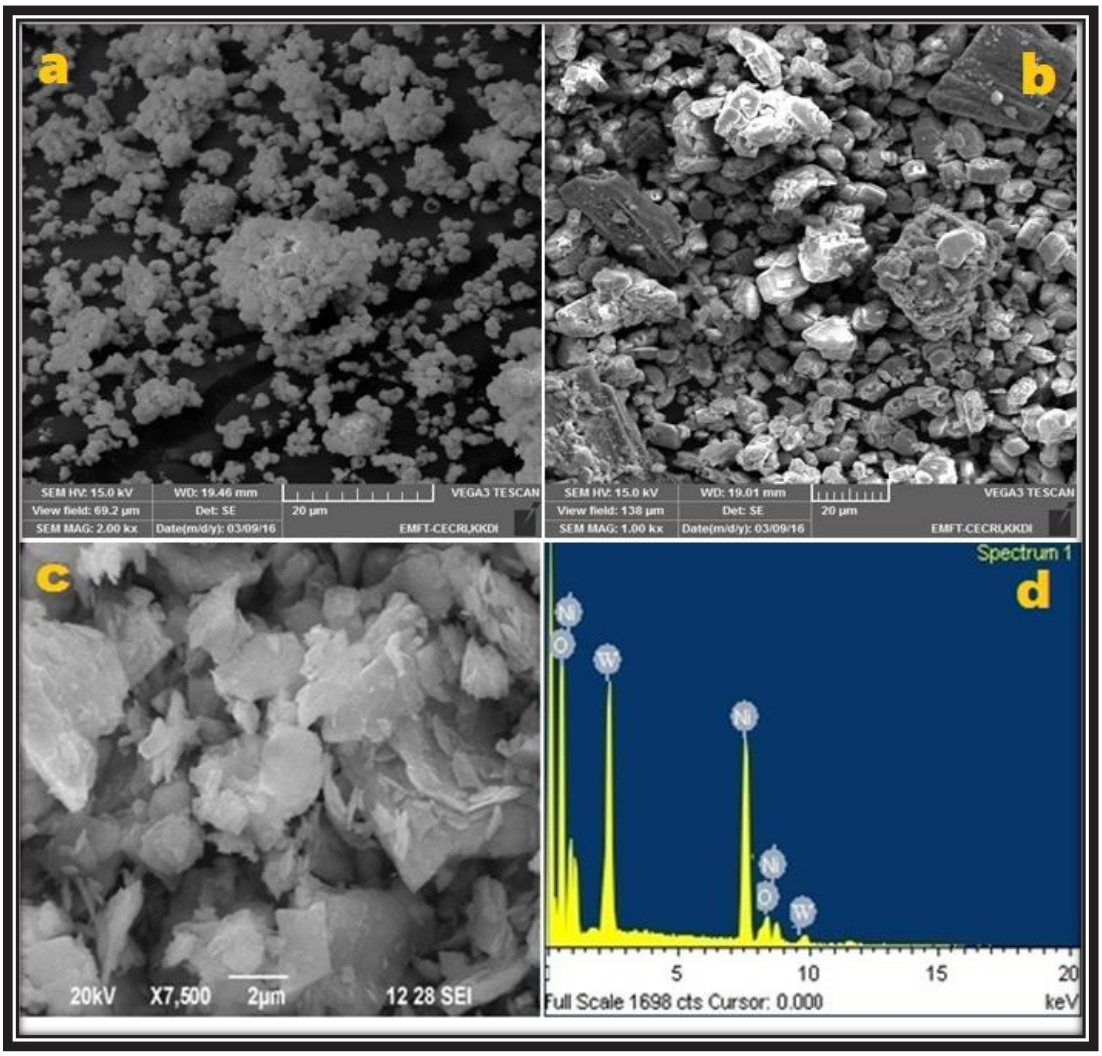

Fig. 4. SEM image of (a) NiO (b)WO_3 (c) 0.5-0.5 mole NiO-WO_3 (d) EDAX image of 0.5-0.5 mole NiO-WO_3

changes in the absorbance profiles of CV solution in the presence of 0.5-0.5 mole NiO-WO_3 nanocomposite was investigated by measuring the degradation of CV at pH 8under visible light irradiation. The control experiments were performed for 30 min under the dark condition in the presence of photocatalytic materials. With the time of irradiation increasing, the peaks at λ_{max} 565nm were reduced quickly and after 180 min of irradiation. At the same time, the blue shift for absorption maximum 565nm can be seen obviously which can be related to de-ethylation process forwarded by the destruction of the skeleton.

The enhanced photocatalytic activity of NiO-WO_3 can be explained as follows: The schematic diagram of electron-hole transfer in NiO-WO_3 was proposed and illustrated in Fig. 7. According to the band edge position, the excited electrons on the conduction band of the p-type NiO transfer to that of the n-type WO_3, and simultaneous holes on the valence band on the n-type WO_3 can be transferred to that of p-type NiO under the potential of the band energy difference. The migration of photogenerated carriers can be promoted by the internal field, so less of a barrier exists. In this case, each majority carrier, electrons in n-type WO_3 and holes in p-type NiO, can migrate easily in the porous semiconductor nanocomposite consisting of small particles, and they enter into recombination between these electrodes. Hence, the electron–hole recombination process is suppressed and the

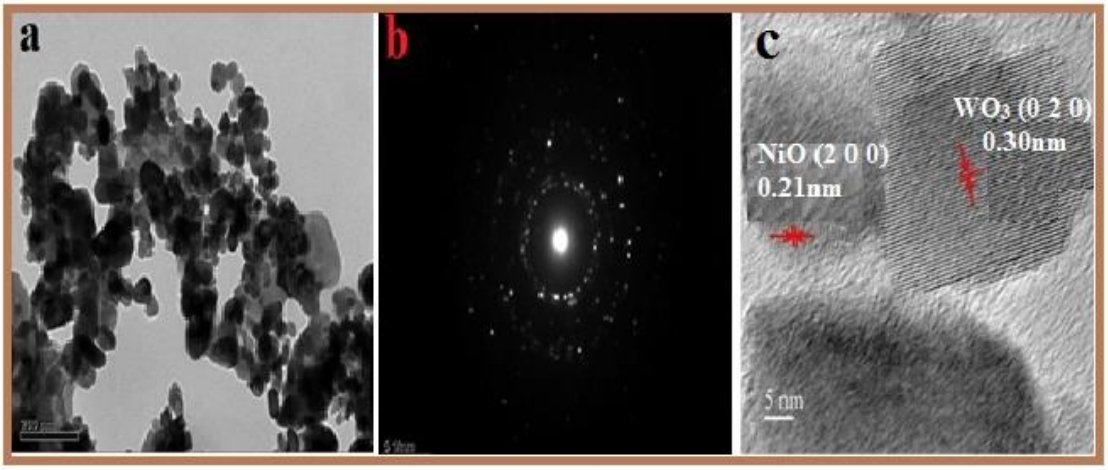

Fig. 5. (a) TEM image of 0.5-0.5 mole NiO-WO_3 (b) SAED pattern of 0.5-0.5 mole NiO-WO_3 (c) HR-TEM images of the 0.5-0.5 mole NiO-WO_3

life time of the charge carriers are extended at the hetero-junction. The electrons accumulated on the CB of WO_3 react with surface adsorbed oxygen to form super oxide radical ($O_2^{\bullet-}$), which further reacts with proton to form super oxide radical (•OH). The reactive species ($O_2^{\bullet-}$, •OH and h^+) formed in the photocatalytic process are highly responsible for the degradation of CV. Therefore, formation of p-n hetero-junction, strong visible light absorption and efficient electron-hole separation could enhance the photocatalytic reaction can be enhanced greatly. The net effect in this case also reduces the energy wasteful recombination of charge carriers and facilitates the photodegradation of organic pollutant [29].

Optimization of reaction parameters

Effect of pH

It was important to study the role of pH on the decolorization of dye .To study the effect of

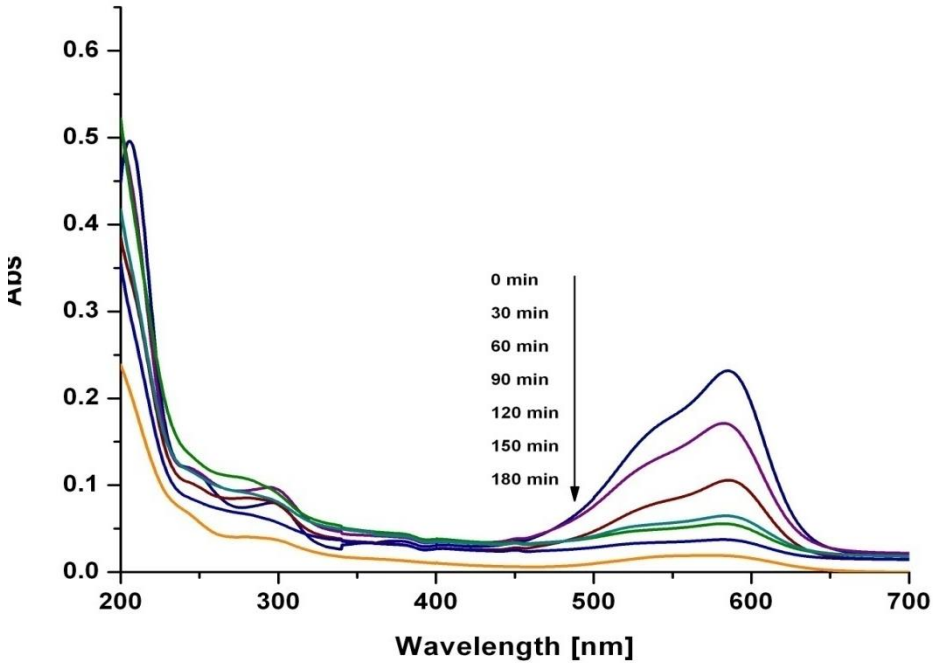

Fig. 6. Time Dependent UV-Vis Spectral Changes of CV (5µM) in Presence of (0.5-0.5 mole NiO-WO_3) (1,5g/L)

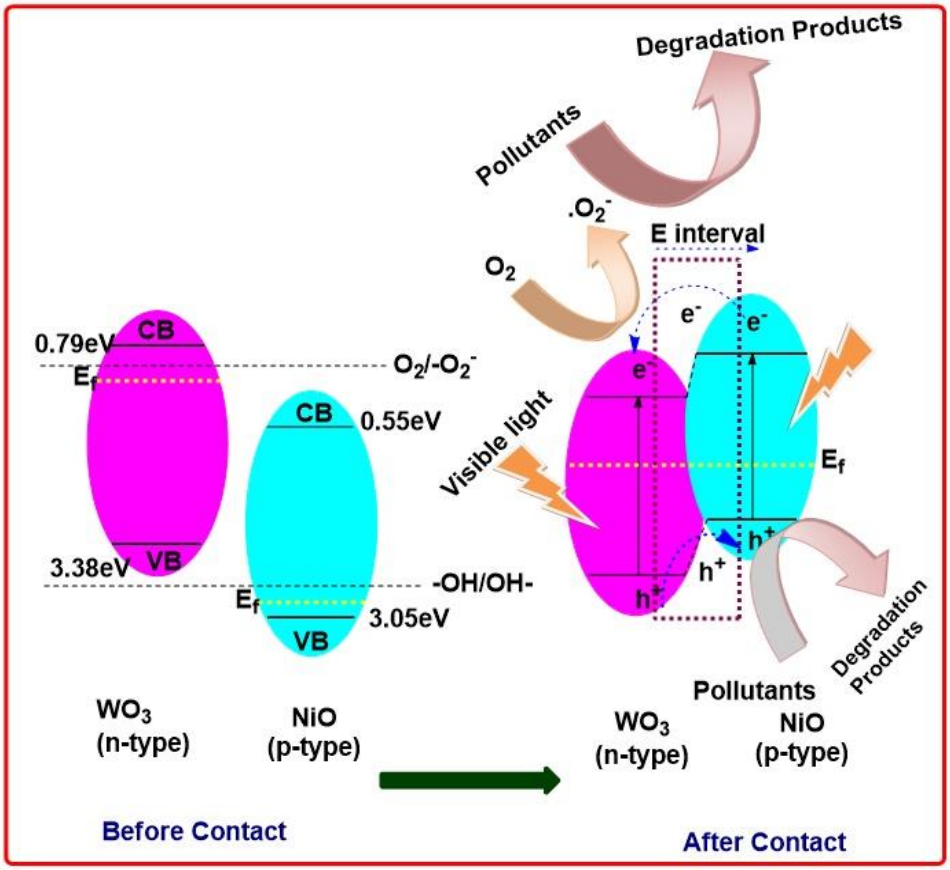

Fig. 7. The schematic diagram of electron transfer in NiO-WO_3 under visible- light irradiation.

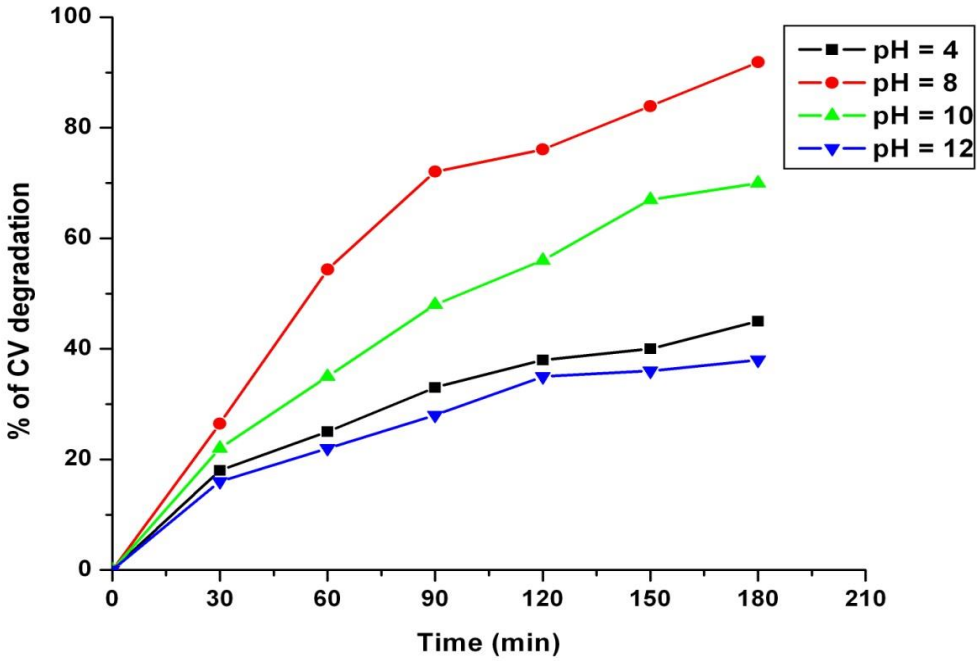

Fig. 8. Effect of pH on the photodegradation of CV

pH on the decolorization efficiency, experiments were carried out at various pH values, ranging from 4-12 for constant dye concentration (5µM) and catalyst dosage (1.25g/L).The Fig. 8 shows the percentage decolorization of CV as a function of pH .It was observed that the decolorization efficiency increases with the increase in pH exhibiting maximum rate of decolorization at pH=8. The presence of large quantities of OH^- ions on the particle surface as well as in the reaction medium favours the formation of OH^- ions which is widely accepted as a principle ,oxidizing species responsible for dye concentration.The percentage efficiency of CV after 180 minutes of irradiation was 92%,64%, 40%, 26% at pH 8,10,4,12 respectively [30-31].

Effect of Catalyst Dosage

The Fig. 9 shows the effect of catalyst dosage on the degradation of CV at pH =8 .It can be seen that the rate of photodegradation increases with increase in the catalyst loading up to 1.25g/L there after the rate of decolorization decreases. Initially an increase in the catalyst dosage increases the total active surface area ,hence the availability of more active sites on the catalyst surface for adsorption and reaction further increase in the amount of the catalyst then decrease the degradation efficacy. The decreased percentage decolorisation at higher catalyst loading may also be due to the activation of activated molecules by collision with ground state molecules. Thus optimum catalyst concentration of 1.25g/L has been employed in order to avoid the excess of catalyst and ensure total absorption of efficient photons. The percentage of CV degradation after 180 minutes of irradiation was 92%,82%, 71%, 64%, 58% 44% at catalyst dosage of 1.25g/L,1 g/L,1.5g/L,0.5g/L,1.75g/L respectively. The results show that optimum catalyst dosage of 0.5-0.5 mole NiO-WO_3 of 1.25g/L in CV degradation was observed [32].

Effect of Concentration

The photocatalytic degradation of CV was carried out by varying the initial concentration of the dye from 5µM to 10µM at pH 8 and 0.5-0.5 mole NiO-WO_3 dosage of 1.25 g/L and the results are shown in Fig. 10. As the concentration of the dye was increased, the percentage of photo decolorization decreased indicating for there to increase the catalyst dose or time span for the

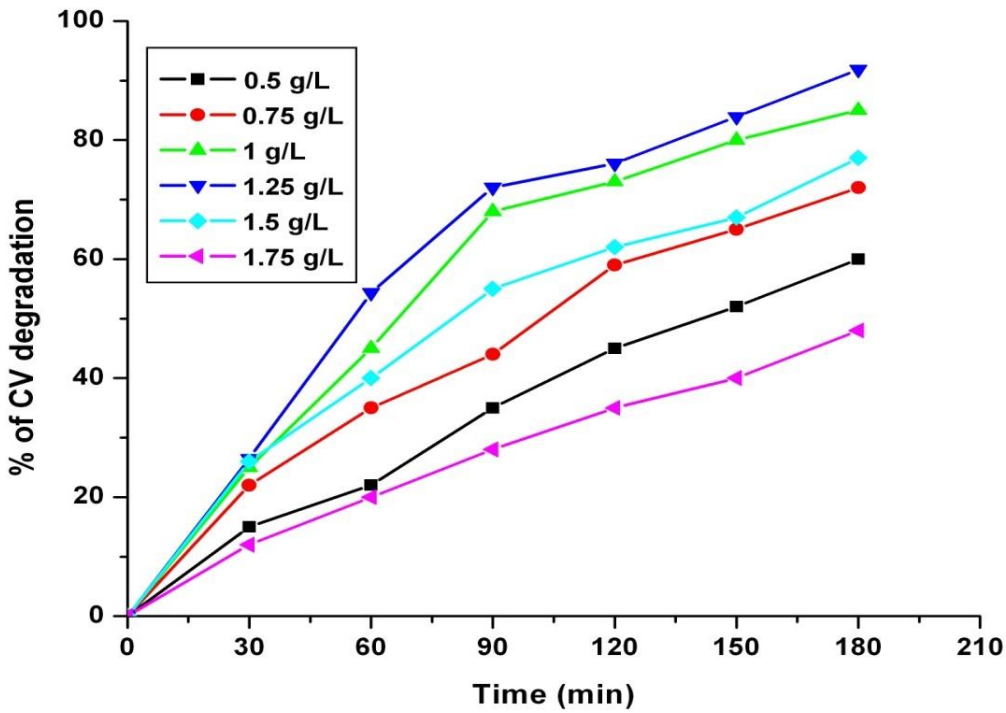

Fig. 9. Effect of catalyst dosage on the photodegradation of CV

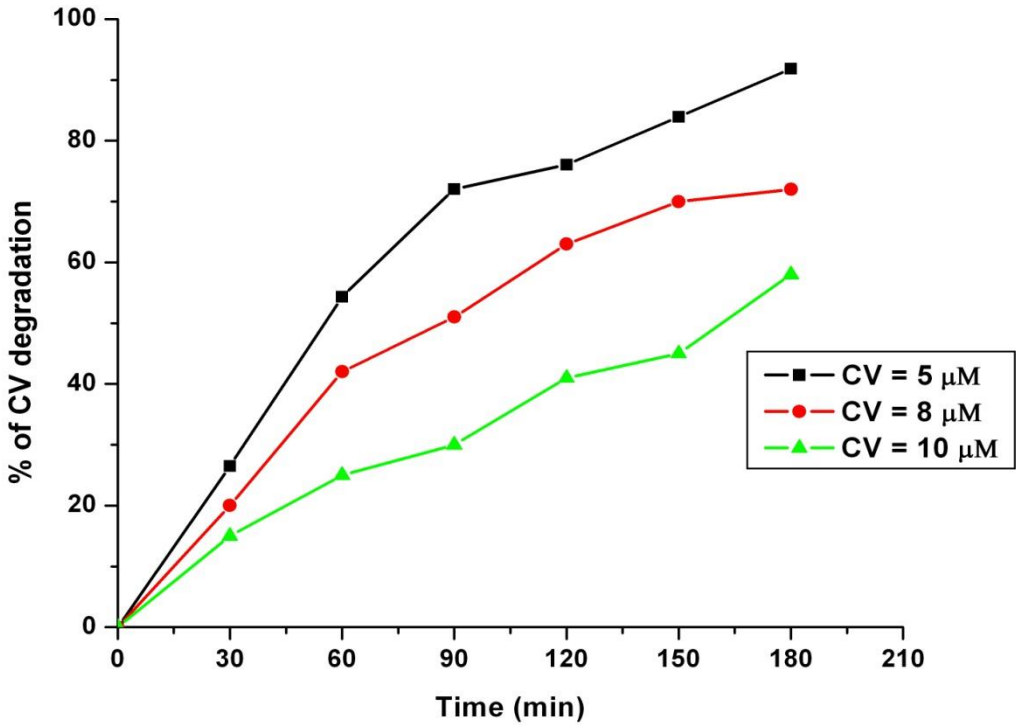

Fig. 10. Effect of concentration on the photodegradation of CV

Table.2. COD removal (mg/L) of CV during photodegradation using 0.5 NiO-0.5 WO_3 under visible light irradiation

Time (Min)	COD removal Efficiency (%) Crystal Violet
0	0
30	14.53
60	22.32
90	41.82
120	57.26
150	79.54
180	92.00

complete removal. The possible explanation for this behavior is that as the initial concentration of dye increases, the path length of the photons entering the solution decreases and in low concentration the reverse effect was observed, thereby increasing the number photon absorption by the catalyst in lower concentration. The degradation efficiency is directly proportional to the probability of the formation of hydroxyl radicals ($OH^{\cdot}$) on the catalyst surface and the probability of ($OH^{\cdot}$) reactivity with the dye molecules. The percentage degradation efficiency of CV after 180 minutes of irradiation was 92%, 70%, 58% at 5 μM,8μM,10μM respectively [33-34].

COD

The COD was used as a measure of the oxygen equivalent of the organic content in a sample that was susceptible to oxidation to carbon-dioxide and water by a strong oxidant. The photocatalytic experiments were performed under ideal conditions. Test samples were collected at every 30 min time interval during the process. The COD of the CV before and after the irradiation of

visible light was estimated and shown in Table. 2. It was observed that the solutions obtained after photodegradation show a significant decrease in COD to 92.00% after 180 min under the optimum conditions. The results revealed that most of organic matter in CV degrades to smaller species (especially inorganic compounds) and hence the required chemically oxygen demand decreases.

CONCLUSIONS

In the present study NiO-WO_3 nanocomposite were successfully synthesized by precipitation deposition method. The prepared photocatalyst was characterized by UV-DRS, FT-IR, XRD, SEM, EDAX and TEM. According to the UV-vis-DRS result the sample shows the absorption edge in the visible region of the spectrum. The photocatalytic activity of 0.5-0.5 mole NiO-WO_3 is found to be more efficient photocatalyst than NiO and WO_3.During3h of simulated under visible light irradiation, 92% of CV (5µM) is degraded using 1.25g/L of0.5-0.5 mole NiO-WO_3. The electron- hole transfer in the p-n hetero-junction is explained schematically through a probable mechanism. The hetero-junctions have good visible light absorption capacity and effectively eliminate the electron-hole recombination. Conclusively, our study proposes a new idea for synthesizing heterogeneous photocatalysts such as NiO-WO_3 which can completely mineralize organic pollutants (CV) help in solving the environmental problems.

ACKNOWLEDGEMENT

The authors thank the Management of Mannar Thirumalai Naicker College for providing necessary laboratory facilities to carry out this work.

CONFLICT OF INTEREST

The authors declare that there is no conflict of interests regarding the publication of this manuscript.

REFERENCES

1. Sajid MM, Khan SB, Shad NA, Amin N, Zhang Z. Visible light assisted photocatalytic degradation of crystal violet dye and electrochemical detection of ascorbic acid using a $BiVO_4/FeVO_4$ heterojunction composite. RSC Advances. 2018;8(42):23489-23498.
2. Nong LX, Nguyen VH, Bach LG, Tran TV, Hong SS, Abdullah B, et al. Crystal violet degradation over $BiVO_4$ photocatalyst under visible light irradiation. Chem Eng Commun. 2019;208(4):530-538.
3. Sawant S, Somani S, Omanwar SK, Somani P. Chemical and Photocatalytic Degradation of Crystal Violet Dye by Indian Edible Chuna (Calcium Oxide/Hydroxide). Journal of Green Science and Technology. 2015;2(1):45-48.
4. Vasic M, Randjelovic M, Momcilovic M, Matovic B, Zarubica A. Degradation of crystal violet over heterogeneous TiO_2-based catalysts: The effect of process parameters. Processing and Application of Ceramics. 2016;10(3):189-198.
5. Shahid M, El Saliby I, McDonagh A, Tijing LD, Kim J-H, Shon HK. Synthesis and characterisation of potassium polytitanate for photocatalytic degradation of crystal violet. Journal of Environmental Sciences. 2014;26(11):2348-2354.
6. Karthik K, Dhanuskodi S, Gobinath C, Prabukumar S, Sivaramakrishnan S. Nanostructured CdO-NiO composite for multifunctional applications. Journal of Physics and Chemistry of Solids. 2018;112:106-118.
7. Wang C, Cheng X, Zhou X, Sun P, Hu X, Shimanoe K, et al. Hierarchical α-Fe_2O_3/NiO Composites with a Hollow Structure for a Gas Sensor. ACS Applied Materials & Interfaces. 2014;6(15):12031-12037.
8. Ding H, Zhu J, Jiang J, Ding R, Feng Y, Wei G, et al. Preparation and gas-sensing property of ultra-fine NiO/SnO_2 nano-particles. RSC Advances. 2012;2(27):10324.
9. Hameed A, Gombac V, Montini T, Graziani M, Fornasiero P. Synthesis, characterization and photocatalytic activity of NiO–Bi_2O_3 nanocomposites. Chem Phys Lett. 2009;472(4-6):212-216.
10. Lin H, Chen Y, Chen Y. Water splitting reaction on NiO/$InVO_4$ under visible light irradiation. Int J Hydrogen Energy. 2007;32(1):86-92.
11. Hameed A, Montini T, Gombac V, Fornasiero P. Photocatalytic decolourization of dyes on NiO–ZnO nano-composites. Photochemical & Photobiological Sciences. 2009;8(5):677.
12. Ku Y, Lin C-N, Hou W-M. Characterization of coupled NiO/TiO_2 photocatalyst for the photocatalytic reduction of Cr(VI) in aqueous solution. J Mol Catal A: Chem. 2011;349(1-2):20-27.
13. Yan J, Gu J, Wang X, Fan Y, Zhao Y, Lian J, et al. Design of 3D WO_3-BN nanocomposites for efficient visible-light-driven photocatalysis. RSC Advances. 2017;7(40):25160-25170.
14. Arai T, Yanagida M, Konishi Y, Iwasaki Y, Sugihara H, Sayama K. Efficient Complete Oxidation of Acetaldehyde into CO_2 over $CuBi_2O_4WO_3$ Composite Photocatalyst under Visible and UV Light Irradiation. The Journal of Physical Chemistry C. 2007;111(21):7574-7577.
15. Leghari SAK, Sajjad S, Chen F, Zhang J. WO_3/TiO_2 composite with morphology change via hydrothermal template-free route as an efficient visible light photocatalyst. Chem Eng J. 2011;166(3):906-915.
16. Huang L, Xu H, Li Y, Li H, Cheng X, Xia J, et al. Visible-light-induced WO_3/g-C_3N_4 composites with enhanced photocatalytic activity. Dalton Transactions. 2013;42(24):8606.
17. Memar A, Phan CM, Tade MO. Photocatalytic activity of WO_3/Fe_2O_3 nanocomposite photoanode. Int J Hydrogen Energy. 2015;40(28):8642-8649.
18. Chakraborty AK, Kebede MA. Preparation and characterization of WO3/Bi_3O_4Cl nanocomposite and its photocatalytic behavior under visible light irradiation. Reaction Kinetics, Mechanisms and Catalysis. 2012;106(1):83-98.

19. Liu L, Zhang Y, Wang G, Li S, Wang L, Han Y, et al. High toluene sensing properties of NiO–SnO_2 composite nanofiber sensors operating at 330°C. Sensors Actuators B: Chem. 2011;160(1):448-454.
20. Raja VR, Muthupandi K, Nithya L. Facile synthesis of heterogeneous CdO-NiO nanocomposite with efficient photocatalytic activity under visible light irradiation. Environmental Chemistry and Ecotoxicology. 2021;3:76-84.
21. Saghatforoush LA, Hasanzadeh M, Sanati S, Mehdizadeh R. $Ni(OH)_2$ and NiO Nanostructures: Synthesis, Characterization and Electrochemical Performance. Bull Korean Chem Soc. 2012;33(8):2613-2618.
22. Santhoshkumar A, Kavitha HP, Suresh R. Preparation, Characterization and Antibacterial Activity of NiO Nanoparticles. Asian J Chem. 2017;29(2):239-241.
23. A P, Arunachalam P, A S, J M, Al-Mayouf AM. Synthesis of $BiFeWO_6/WO_3$ nanocomposite and its enhanced photocatalytic activity towards degradation of dye under irradiation of light. Colloids Surf Physicochem Eng Aspects. 2018;559:83-91.
24. Liu Z, Zhao Z-G, Miyauchi M. Efficient Visible Light Active $CaFe_2O_4/WO_3$ Based Composite Photocatalysts: Effect of Interfacial Modification. The Journal of Physical Chemistry C. 2009;113(39):17132-17137.
25. Dorneanu PP, Airinei A, Olaru N, Homocianu M, Nica V, Doroftei F. Preparation and characterization of NiO, ZnO and NiO–ZnO composite nanofibers by electrospinning method. Materials Chemistry and Physics. 2014;148(3):1029-1035.
26. Manjunatha AS, Pavithra NS, Shivanna M, Nagaraju G, Ravikumar CR. Synthesis of Citrus Limon mediated SnO_2-WO_3 nanocomposite: Applications to photocatalytic activity and electrochemical sensor. Journal of Environmental Chemical Engineering. 2020;8(6):104500.
27. Ramasamy Raja V, Karthika A, Lok Kirubahar S, Suganthi A, Rajarajan M. Sonochemical synthesis of novel $ZnFe_2O_4/CeO_2$ heterojunction with highly enhanced visible light photocatalytic activity. Solid State Ionics. 2019;332:55-62.
28. Lin X, Liu C, Wang J, Yang S, Shi J, Hong Y. Graphitic carbon nitride quantum dots and nitrogen-doped carbon quantum dots co-decorated with $BiVO_4$ microspheres: A ternary heterostructure photocatalyst for water purification. Sep Purif Technol. 2019;226:117-127.
29. Feng X, Wang P, Hou J, Qian J, Wang C, Ao Y. Oxygen vacancies and phosphorus codoped black titania coated carbon nanotube composite photocatalyst with efficient photocatalytic performance for the degradation of acetaminophen under visible light irradiation. Chem Eng J. 2018;352:947-956.
30. Amano F, Ishinaga E, Yamakata A. Effect of Particle Size on the Photocatalytic Activity of WO_3 Particles for Water Oxidation. The Journal of Physical Chemistry C. 2013;117(44):22584-22590.
31. Uddin MM, Hasnat MA, Samed AJF, Majumdar RK. Influence of TiO_2 and ZnO photocatalysts on adsorption and degradation behaviour of Erythrosine. Dyes and Pigments. 2007;75(1):207-212.
32. Ghiyasiyan-Arani M, Masjedi-Arani M, salavati-Niasari M. Size controllable synthesis of cobalt vanadate nanostructures with enhanced photocatalytic activity for the degradation of organic dyes. J Mol Catal A: Chem. 2016;425:31-42.
33. Hou J, Wang Z, Jiao S, Zhu H. Bi_2O_3 quantum-dot decorated nitrogen-doped Bi_3NbO_7 nanosheets: in situ synthesis and enhanced visible-light photocatalytic activity. CrystEngComm. 2012;14(18):5923.
34. Cao J, Xu B, Lin H, Luo B, Chen S. Novel heterostructured Bi_2S_3/BiOI photocatalyst: facile preparation, characterization and visible light photocatalytic performance. Dalton Transactions. 2012;41(37):11482.